RESEARCHERID
THOMSON REUTERS

[Amarasooriya* 6(9): September, 2019] ISSN 2349-4506
Impact Factor: 3.799

Global Journal of Engineering Science and Research Management

LABORATORY SCALE FIXED-BED COLUMN ADSORPTION STUDY OF METHYLENE BLUE ON GLUTARALDEHYDE CROSS-LINKED CHITOSAN BEADS

M. P. N. A. Amarasooriya*[1], C. S. K. Rajapakse[2]
*[1,2]Department of Chemistry, Faculty of Science, University of Kelaniya, Kelaniya 11600, Sri Lanka

DOI: 10.5281/zenodo.3452554

KEYWORDS: Adsorption, methylene blue, glutaraldehyde cross-linked chitosan beads, fixed –bed column, breakthrough curves, kinetic models.

ABSTRACT

This work focuses on the exploration of the potential of glutaraldehyde cross-linked chitosan beads (GCLCBs) to remove methylene blue (MB) from aqueous solutions using bench-scale fixed bed columns. The biosorbent, GCLCB was prepared using glutaraldehyde as the croos-linking agents and characterized by SEM and FTIR. A down-flow bench-scale fixed-bed column packed with GCLCBs were designed for column studies. The effects of adsorbent bed height (1, 2 and 3 cm), inlet flow rate (5, 10 and 15 mL/min) and initial MB concentration (10, 12 and 15 mg/L) on the column performance were analyzed using breakthrough curves. The maximum adsorption capacity (225.47 mg/g) of MB was observed at 3 cm bed height, inlet flow rate of 5 mL/min and at initial MB concentration of 12 mg/L. The breakthrough curves were further analyzed using three common kinetic models namely the Thomas, Yoon – Nelson, and Adams - Bohart models to determine the column adsorption kinetic parameters. Thomas model showed that the value of equilibrium adsorbate uptake (q°) increased with increasing all three process parameters. Yoon – Nelson model showed that the time required for achieving 50% adsorbate breakthrough, τ agreed well with the experimental data (τ_{exp} 50%) in the entire column system. The results of the kinetic models revealed that both the Thomas and Yoon – Nelson models were fitted well with the experimental data.

INTRODUCTION

Many dyes are organic compounds and which are widely used in industries such as the textile, food, pulp mill, paper, pharmaceutical, printing, photographic, leather, electroplating plastics,[1] etc. Different varieties of synthetic dyes are available in the market in all over the world [1,2,3] and the total annual global colorant production is 800,000 tons of which approximately 15% of the used dyes are released into the environment through wastes by various industrial sources [4]. Dye-containing waste effluent is a big threat not only to the environment, but also to human life as most of these are toxic, mutagenic, or carcinogenic [5]. Therefore, economical removal of dyes from wastewater has become a significant issue and an environmental challenge in nowadays. Various physical, chemical and biological treatment methods including ion exchange, chemical precipitation, coagulation, adsorption, flocculation, reverse osmosis, advanced oxidation, ozonation, membrane filtration, photocatalytic degradation, liquid–liquid extraction, biological degradation, etc have been widely used for the treatment of dye-bearing wastewater [6,7]. Unfortunately, most of these processes have significant major drawbacks such as high cost, incomplete removal, high-energy requirements, generation of toxic sludge, etc. [6] Even though dye and pigment adsorption onto activated carbon, has proven to be one of the most effective treatment methodologies for removal of dyes from waste effluents, high production cost of activated carbon limit its use as an adsorbent for the removal of pollutants [7,8, 9]. Therefore, the research on use of biodegradable, non-toxic, readily available natural polymers as cost- effective adsorbents has intensified in recent years. The dye adsorption capabilities of natural material such as pine cone [8], *Moringa oleifera* seeds [10], leaves of *Nymphya* [11] rice husk[12], jack fruit leaf powder[13], coconut shell [14] like plant based materials were previously investigated. But one of the drawbacks of use of these material as adsorbents is their unavailability in all geographical areas [15]. In addition, potential of using several other natural materials such as peat, wood chips, cucurbituril chitosan as adsorbents have also been investigated [6].

Chitosan, (poly-2-amino-2-deoxy-β-(1, 4)-D-glucopyranose) is derived from Chitin (poly-2-acetamide-2-deoxy-β-(1, 4)-D-glucopyranose) which is the second most abundant biopolymer in nature after cellulose [15]. Chitin is

found in exoskeleton of crustaceans, marine arthropods, some seaweed and yeasts [16]. One of the value added product of chitin is chitosan and which can be produced by deacetylation of chitin. Chitosan being a bio-polymer is readily available, biodegradable, nontoxic[16,17] and it has a wide variety of applications[18] in different fields such as pharmaceuticals [19,20,21], food [22,23], cosmetics [24], biotechnology [25], paper[26] agriculture [27], etc. As chitosan has ability to adsorb different pollutants, it is widely used in wastewater treatment industries to remove heavy metal ions [28], dyes [16], fluoride [29, 30], phosphate [9] like anions, sediment particles [31, 32] etc., from the wastewaters. Many pollutants become bound by physical and/or chemical interactions because chitosan has ability to form hydrogen bonds, Van der Waals forces and coordination bonds (chelation) with the pollutants depending on the pH of the solution. Nevertheless, chitosan has poor chemical stability in acidic solutions. Also, chitosan may aggregate in solution and which will reduce its sorption ability. Hence, its application is limited and chitosan needs to be modified to improve its chemical stability and adsorption capabilities [9]. For this purpose, chitosan has been both physically and chemically modified to alter its properties to suit various applications. The adsorption performance of chitosan flakes (raw chitosan) can be enhanced by physically modifying it to form membranes [16,33], beads [16,34,35] ,films[16], nano particles [36,37], fibers [28,38], hollow fibers [39] and sponge honey comb [40] etc. Chitosan is chemically modified to improve the adsorption capacity by introducing relevant functional groups to enhance the chemisorption and to increase the chemical stability. Methods of chemical modification include crosslinking [16], grafting [16], and surface impregnation of chitosan [16].

In this study, physically modified chitosan beads were chemically modified using glutaraldehyde as the cross-linking agent to produce glutaraldehyde cross-linked chitosan beads (GCLCBs) for the removal of model cationic dye methylene blue (MB) (figure 1). Here, the cross-linking agent; Glutaraldehyde (figure 2) introduces intermolecular bridges between chitosan macromolecules which may lead to the enhancement of the chemical stability, mechanical strength and adsorption capacity of chitosan.

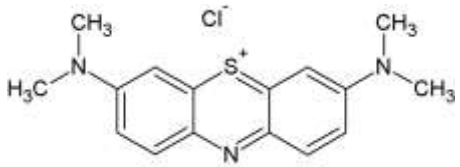

Figure 1 – The structure of Methylene Blue (MB)

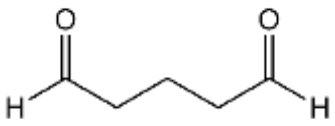

Figure 2 – The structure of Glutaraldehyde, the cross-linking agent

The aim of this study was to investigate the potential of physically and chemically modified chitosan, GCLCBs to remove MB from aqueous solutions using bench-scale fixed bed columns under different column processing conditions, and analyze the corresponding breakthrough curves using the Thomas, Yoon – Nelson and Adams–Bohart mathematical kinetic models to determine the column adsorption kinetic parameters.

MATERIALS AND METHODS

Medical grade chitosan was purchased from PT, Biotecsurindo, Cireban, West java, Indonesia (Average molecular weight = 191000 g/mol, deacetylation percentage = 80- 85%, purity = 95 %, solubility = over 99 % in 1 % acetic acid). Glutaraldehyde (80 wt%, MW=100.12) was used as the cross-linking agent. Methylene blue, MB (RIEDEL-DE HAENAG-Germany, MW=319.86 g/mol was selected as the model cationic dye for the adsorption studies. All other chemicals used were analytical grade. Deionized water was used to prepare all solutions.

Preparation of glutaraldehyde cross-linked chitosan beads (GCLCBs)

Chitosan solution (3% w/v) was prepared by dissolving chitosan in acetic acid (2.0 % v/v). Next, the chitosan solution was added from a pipette, drop by drop into a NaOH (0.50 M) bath to form chitosan beads. The chitosan beads were soaked in NaOH solution (0.50 M) for 24 hours and rinsed with distilled water to adjust the pH to 7. The prepared chitosan wet beads were cross-linked by soaking the beads in glutaraldehyde solution (80 wt %) for 48 hours and then glutaraldehyde cross-linked chitosan beads (GCLCB) were washed with deionized water to remove any free glutaraldehyde and beads were then soaked in deionized water until further use.

Preparation of methylene blue (MB) solutions

A stock solution of MB at a concentration of 1000 mg/L was prepared by dissolving 0.1 g of dye in deionized water and it was diluted to prepare the solutions with required concentrations for the experiment.

Characterization of the adsorbent, GCLCB

The surface morphology of GCLCBs was analyzed before and after adsorption of MB by Scanning Electron Microscopy (VEGA3 SEM, TESCAN). Fourier Transformation Infrared (FTIR) spectra of chitosan, GCLCBs and MB adsorbed GCLCBs were obtained by FTIR Spectroscopy (Bruker, Alpha-T, Germany) using Attenuated Total Reflection (ATR) method.

Fixed-bed column adsorption studies

Column adsorption studies were conducted by designing a column as shown in figure 3. A glass column with 25.5 cm in height and 5 cm in internal diameter was packed with the prepared adsorbent, GCLCB to desired height and it was operated under down flow at room temperature.

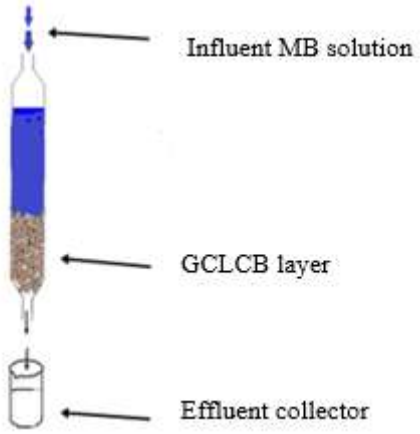

Figure 3: Schematic diagram of the design column

To determine the effect of bed height, inlet flow rate, and initial MB concentration on column adsorption performance, laboratory scale column adsorption studies were first conducted. The effect of initial bed height on MB adsorption was examined by changing the bed height (1 cm, 2 cm and 3 cm of GCLCB) with 10 mg/L initial dye concentration, and 5 mL/min inlet flow rate at room temperature ($30 \pm 2\ ^0$C). The effect of flow rate on MB adsorption was studied by changing the flow rate (5, 10, 15 mL/min) with 3 cm bed height, and 10 mg/L initial dye concentration at room temperature ($30 \pm 2\ ^0$C). The effect of initial adsorbate concentration on MB adsorption was investigated by varying the initial MB concentration (10, 12 and 15 mg/L) with 3 cm bed height of the adsorbent, and 5 mL/min flow rate at room temperature ($30 \pm 2\ ^0$C). The effluent leaving the bottom of the column was collected at regular time intervals and MB concentration of the effluent was determined by measuring the absorbance at 665.0 nm using a UV-Visible Spectrophotometer (Agilent Technologies, Cary 60).

Modeling of the breakthrough curves

The column performance was examined by assessing the corresponding breakthrough curves (BTC), which were obtained from the plot of C/Co versus time t, where C and Co are the outlet MB dye and initial MB inlet concentrations in mg/L, respectively. The breakthrough time (t_b), time required for full bed exhaustion (t_t), experimental uptake capacity ($q_{e(exp)}$), length of used bed height(H_b) and length of unused bed (H_{UNB}) were determined at each column operating conditions. Based on the results the best conditions for MB removal by the designed column was determined. Further, the obtained experimental BTCs under various column processing conditions were fitted with three common kinetic models namely the Thomas model, Yoon – Nelson model and Adams – Bohart model to determine the fixed-bed column adsorption kinetic parameters important in designing large-scale columns in water purification systems.

Statistical analysis

All experiments were carried out in duplicates and results were reported as mean ± standard deviation. MATLAB software was used to find the area of breakthrough curves.

RESULTS AND DISCUSSION

Preparation and characterization of GCLCB

Figure 4, (a) and (b) shows the prepared chitosan beads (CB) and GCLCB respectively. GCLCB were spherical in shape with mean diameter of 4.00±0.02 mm.

(a) ***(b)***

Figure 4: (a) Chitosan beads and (b) GCLCB

As the adsorption of GCLCB depends on the porosity and the surface functional groups of the adsorbent, surface morphology of the adsorbent was examined by SEM and it was further characterized by FTIR.

SEM analysis

Figure 5, (a) and (b) represent surface morphology of GCLCBs before and after adsorption of MB respectively.

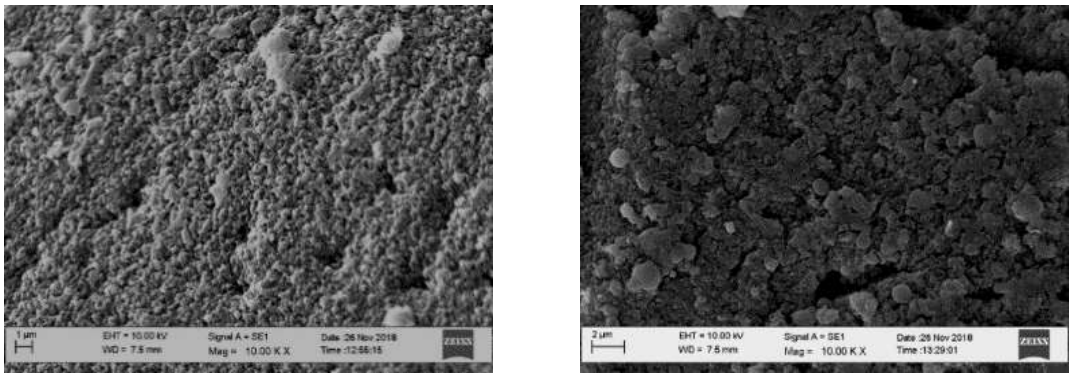

(a) (b)

Figure 5 – SEM micrographs of GCLCBs (a) before and (b) after adsorption of MB (Mag=10.00K)

The SEM analysis revealed that GCLCBs have highly porous structures with irregular surface. The observed less porous, smooth surface of MB treated GCLCBs could be due to adsorbed bulky MB ions filling the pores that existed before adsorption studies.

FTIR analysis

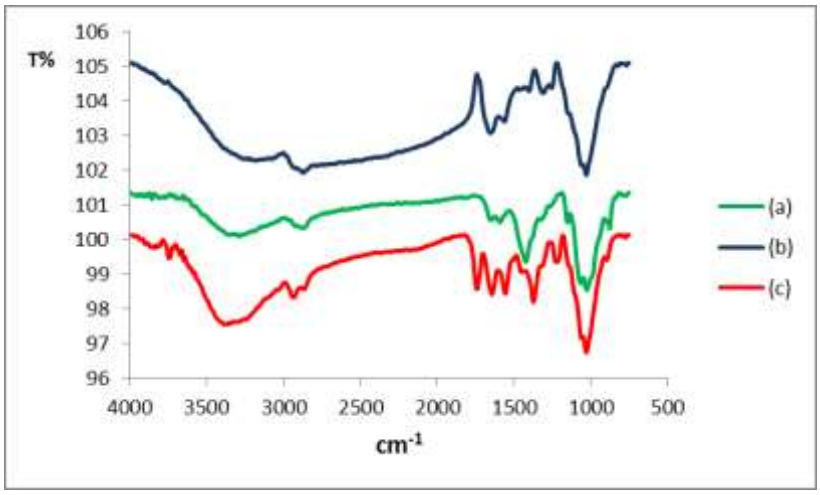

Figure 6 – FTIR spectra for (a) Chitosan (b) GCLCB (c) GCLCB after adsorption of MB

Fig. 6 shows the FTIR spectra of (a) chitosan (b) GCLCB and (c) MB adsorbed GCLCB in the 750-4000 cm^{-1} wavenumber range. The main bands of IR spectrum of chitosan include, a strong broad band at the wavenumber region 3250–3400 cm^{-1} which corresponds to N-H and O-H stretching vibrations and intra-molecular hydrogen bonds [41]. The bands appear at around 2926 cm^{-1} and 2865 cm^{-1} correspond to C-H symmetric stretching and C-H asymmetric stretching respectively. Bands at around 1652 cm^{-1} and 1591 cm^{-1} can be attributed to the C=O stretching of N-acetyl groups [41] and N-H bending vibration of the primary amine [41]. As shown in Fig. 6 (b), chitosan after the modification to form GCLCB, the stretching vibration was shifted to lower wave number of 3197 cm^{-1} which was originally appeared at around 3286 cm^{-1} corresponded to stretching of –O-H and $–NH_2$ groups indicating that the cross-linking by glutaraldehyde affects the normal vibration scheme of chitosan. In the spectrum of GCLCB, a band corresponds to -N-H bending vibrations of primary amine groups at 1591 cm^{-1} has disappeared. This may be shifted and overlapped by other bands after cross-linking. As shown in Fig. 6 (c), upon biding of MB, the intensity of the bands in IR spectrum of GCLCB, which correspond to –O-H and $–NH_2$ stretching vibrations were increased getting broaden and shifted to a higher frequency suggesting that there may be interactions between MB ions and the functional groups (-O-H/N-H) in GCLC. As shown in figure 6 (c) IR vibrational bands appeared at 1745 and 1639 cm^{-1} can be attributed to the $=N^{+}(CH^{3})$ group of MB and which indicate the presence of adsorbed MB on GCLCBs. Similar observation was reported in MB adsorbed chitosan clay composite [42].

Continuous flow fixed-bed column adsorption studies

MB adsorption performance of fixed-bed column packed with GCLCB under different column processing conditions (at different bed heights, inlet flow-rate and initial MB concentration) was analyzed using the breakthrough curves (BTCs).

Breakthrough curves

A schematic diagram of a typical breakthrough curve (BTC) is usually expressed in terms of ratio of outlet adsorbate concentration (C) to the inlet adsorbate concentration (C_0) i.e. (C/C_0) as a function of time, t. is shown in figure 7.

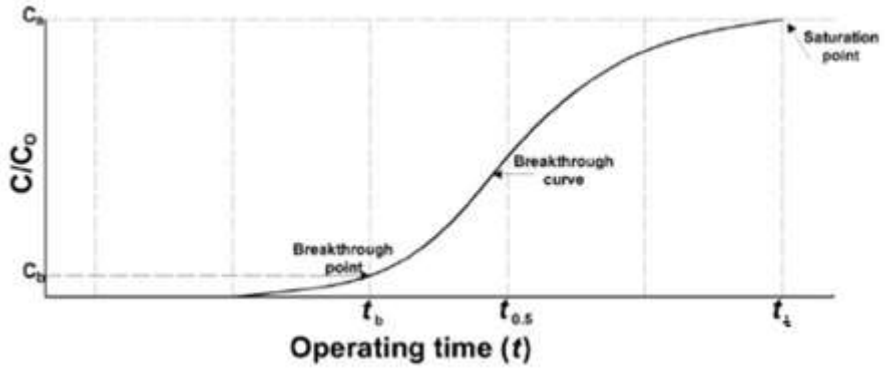

Figure 7: A schematic diagram of a typical breakthrough curve

BTCs can be used to calculate important column parameters as follows; [8, 43]
The unused bed height (H_{UNB}) can be calculated as;

$$H_{UNB} = (1- t_b/t_t)\ H_T \quad (1)$$

Where, H_T = Total bed height/cm, t_t = Time required for full bed exhaustion/min,
t_b = Breakthrough time/min. The breakthrough point occurs when the 0.10 C/C_0 adsorbate's concentration starts to leave the column.
The used bed height (H_b) is given as;

$$H_b = (t_b/t_t)\ Ht \quad (2)$$

The total effluent volume (V_{eff}) can be calculated as;

$$V_{eff} = Q\ t_t \quad (3)$$

Where, Q = Volume flow rate / mL/min
The total adsorbed MB quantity (q_{total}) in the column for a given adsorbate concentration and flow rate is given as;

$$q_{total} = QA/1000 \quad (4)$$

Where A = Area above the breakthrough curve
The experimental adsorption capacity (mg g^{-1}), $q_{e(exp)} = q_{total}/X$ (5)
where X= dry weight of adsorbent(g)
The total amount of MB dye sent to column (m_{total}) can be calculated as;

$$m_{total} = C_0\ Q\ t_{total}\ /1000 \quad (6)$$

Column adsorption performance at various operating conditions
Effect of bed height
BTCs plotted at different bed heights (h) at constant MB inlet flow rate of 5 mL/min and initial MB inlet concentration of 10 mg/L and shown in figure 8 and parameters obtained from BTCs are tabulated in table 1.

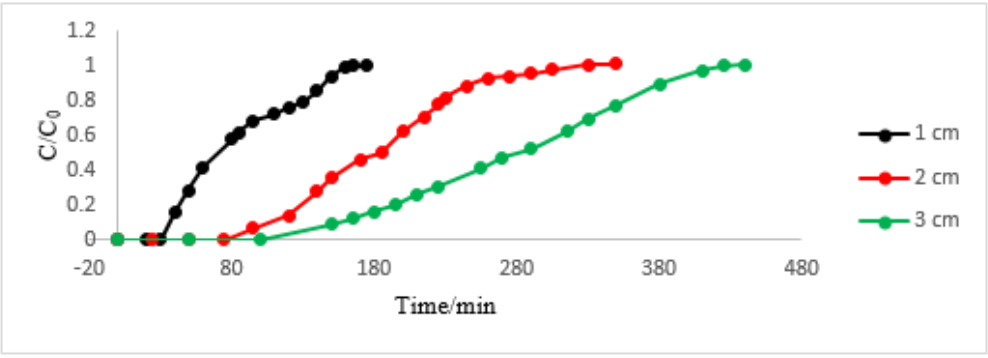

Figure 8: BTCs for adsorption of MB onto GCLCB at different bed heights, (initial MB concentration 10 mg/L, 5 mL/min flow rate and temperature 30±2 °C)

Table 1; Parameters obtained from BTCs of packed-bed column for MB adsorption onto GCLCB at different bed heights

H_t (cm)	t_b (min)	V_{eff} (mL)	t_t (min)	m_{total} (mg)	q_{total} (mg)	$q_{e(exp)}$ (mg/g)	H_{UNB} (cm)	H_b(cm)
1	35	410	165	80.50	74.28	90.59	0.79	0.21
2	90	825	330	162.00	184.58	155.11	1.455	0.545
3	130	1075	425	211.08	224.49	181.04	2.08	0.92

According to the graphs, the slope and the shape of BTCs were varied as the bed height of the adsorbent was varied at constant inlet MB concentration of 10 mg/L and an inlet flow rate of 5 mL/min. t_b was increased as the bed height was increased from 1 to 3 cm. As bed height is increased, more adsorbent surface exposed to the adsorbate, providing more binding sites for MB adsorption. Hence, MB dye removal by the adsorbent also increases. Further, the experimental adsorption capacity $q_{e(exp)}$) is also increased from 90.59 to 181.08 mg/g and used bed height (H_b) also increased from 0.21 to 0.92 cm as the bed height is increased.

Effect of inlet flow rate

The effect of inlet flow rate on MB adsorption performance of a column packed with GCLCBs was studied by varying flow rate as 5, 10 and 15 ml/min at initial inlet MB concentration of 10 mg/L, and bed height of 3 cm and the corresponding BTCs are depicted in figure 9. The parameters obtained from the BTCs are tabulated in table 2.

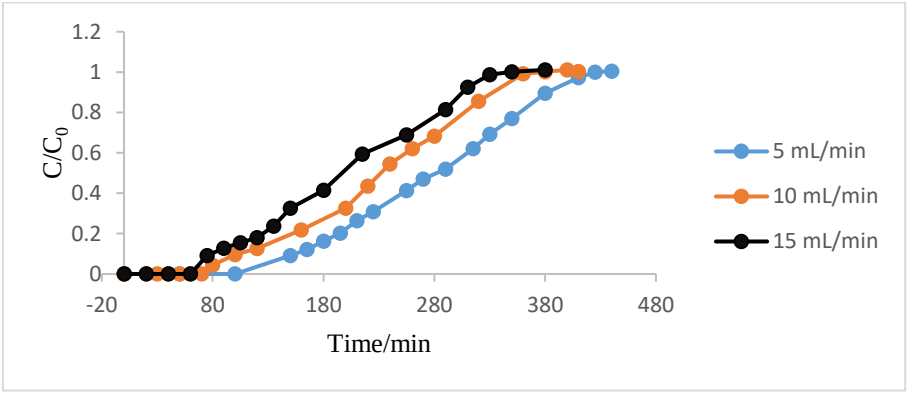

Figure 9 – BTCs for adsorption of MB onto GCLCB at different inlet flow rates (10 mg/L initial MB concentration, 3 cm bed height and temperature 30±2 °C)

Table 2; Parameters obtained from BTCs of packed-bed column for MB adsorption onto GCLCB at different flow rates

Flow rate (mL/min)	t_b (min)	V_{eff} (mL)	t_t (min)	m_{total} (mg)	q_{total} (mg)	$q_{e(exp)}$ (mg/g)	H_{UNB} (cm)	H_b (cm)
5	130	1075	425	211.08	224.49	181.04	2.08	0.92
10	80	560	380	109.97	104.04	83.90	2.37	0.63
15	70	475	350	93.27	77.68	62.65	2.40	0.60

As tabulated in table 2, t_b was decreased from 130 to 70 min when increasing the flow rate from 5 to 15 ml/min. Therefore, the results revealed that the breakthrough occurred faster with higher flow rate and this may be due to the fact that increasing flow rate does not give sufficient time for adsorabte molecules to interact with the binding

sites of the adsorbents. Further, $q_{e(exp)}$ was also decreased with increasing inlet adsorbate flow rate. Similar type of results was reported in literature for different types of adsorbents [8, 44]

Effect of initial MB concentration

Similarly, the effect of initial inlet MB concentration on column performance was investigated by varying the initial MB concentration (C_o) as 10, 12 and 15 mg/L and the corresponding BTCs, parameters obtained from BTCS are given in figure 10 and table 3 respectively.

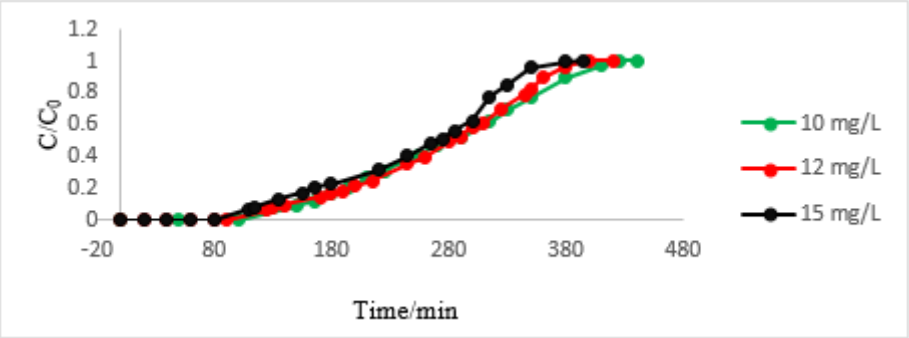

Figure 10 – BTCs for adsorption of MB onto GCLCB at different initial MB concentrations (5 mL/min flow rate, 3 cm bed height and temperature= 30±2 ˚C)

Table 3; Parameters obtained from BTCS of packed-bed column for MB adsorption onto GCLCB at different initial MB concentrations

Concentations(C_0) (mgL^{-1})	t_b (min)	V_{eff} (mL)	t_t (min)	m_{total} (mg)	q_{total} (mg)	$q_{e(exp)}$ (mg/g)	H_{UNB} (cm)	H_b (cm)
10	130	1075	425	211.08	224.49	181.04	2.08	0.92
12	115	1000	400	235.63	279.58	225.47	2.138	0.862
15	100	950	380	279.80	207.28	167.16	2.21	0.79

According to the results, t_b value was decreased with increasing initial inlet MB concentration because available sites are quickly filled at higher MB concentration resulting in reduced t_b. Similar type of observations were reported for adsorption studies in pinecone activated carbon, peanut husk and *Mangoatana garcinia* peel based granular activated carbon [8, 45, and 46].

Kinetic modelling of fixed-bed column breakthrough curves

Various kinetic models namely Thomas, Yoon – Nelson and Adams – Bohart models have been used to analyze the breakthrough curves to describe the column performance, and to predict the behavior of the column, and also to determine the column kinetic parameters and adsorption capacity of the fixed-bed columns in different systems. [8, 43, 44, 47]

Thomas model

Thomas model assumes that the process follows Langmuir kinetics of adsorption–desorption with no axial dispersion, and the driving force follows second order reversible reaction kinetics (8, 43, 44, 47). The linearized form of the Thomas model is given as equation 7.

$$\ln\left(\frac{Co}{Ci}-1\right)=\left(\frac{KTqom}{Q}\right)-\left(\frac{KTCoV}{Q}\right) \quad (7)$$

Where,

KT- Thomas rate constant (mL/mg min)
q_0 – Maximum adsorption capacity (mg/g)
m - The amount of adsorbent in the column (g)
C_0 –Inlet initial concentration (mg/L)
C - Effluent MB concentration (mg/L)
Q - Flow rate (mL/min)
V - Effluent volume (ml)
KT and q_0 can be determined from the plot of ln [(Co/C) −1] vs. t at a given flow rate.

Yoon–Nelson model

Yoon-Nelson model is a simple model and it does not require any data related to the characteristics of adsorbate, the type of adsorbent and the physical properties of the adsorption bed (8,44). This model assumes that the rate of decrease in the probability of adsorption for each adsorbate molecule, is proportional to the probability of adsorbate adsorption and the probability of adsorbate breakthrough on the adsorbent (8,44). The linearized form of the Yoon-Nelson expression for a single component system is given as equation 8 (8,44,47).

$$ln\left(\frac{C}{Co-C}\right) = Kt - K\tau \quad (8)$$

Where,
K - Yoon and Nelson rate constant (min^{-1})
Co -Inlet or initial concentration (mg/L)
C - MB concentration in the effluent (mg/L)
t -Sampling time (min)
τ -Time required for 50% adsorbate breakthrough (min)
K and τ can be determined from the slope and intercept respectively from the plot of ln [C/ (C_0 −C)] vs. sampling time (t)

Adams–Bohart model

The Adam–Bohart model assumes that the adsorption rate is proportional to both the residual capacity of the adsorbent and the concentration of the adsorbing species. This model is used for the description of the initial part of the breakthrough curve (43, 44, 47). The linearized form of the Adam–Bohart equation is expressed as,

$$\ln\left(\frac{C}{Co}\right) = kCot - \frac{kNoZ}{Uo} \quad (9)$$

Where,
k = Adam–Bohart kinetic constant (L/mg min)
No = Saturation concentration/maximum adsorption capacity (mg/L)
Z = the bed depth of column (cm)
Uo = Linear velocity (cm/min)
Co -Inlet or initial concentration (mg/L)
C - MB concentration in the effluent (mg/L)
k and No can be obtained from a plot of ln (C/Co) versus t.
In this study, the breakthrough curves obtained under different column processing conditions were analyzed with the mathematical models of Thomas, Yoon- Nelson and Adams–Bohart kinetic models.

Breakthrough curve analysis by the Thomas model at different bed heights, inlet flow rates and initial MB concentrations

Thomas plots at different bed heights, flow rates and initial concentrations are shown in figure 11, 12 and 13 respectively and kinetic parameters obtained from these models under the given conditions are shown in table 4.

ISSN 2349-4506
Impact Factor: 3.799
Global Journal of Engineering Science and Research Management

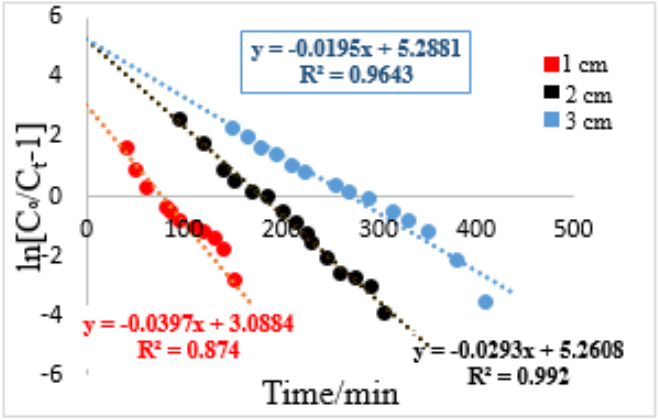

Figure 11 – Thomas plots for the adsorption of MB onto GCLCB at different bed heights (initial MB dye concentration 10 mg/L, inlet flow rate 5 mg/L and temperature 30±2 ˚C)

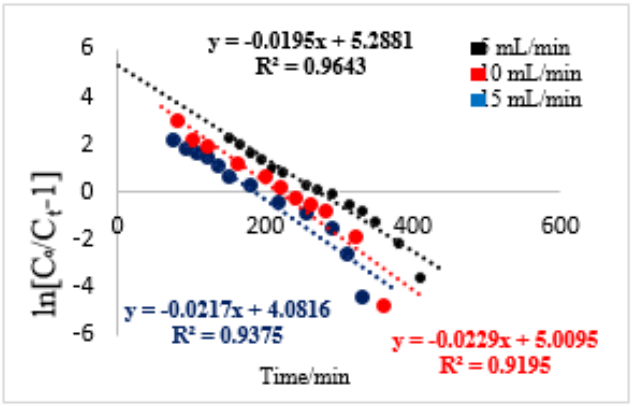

Figure 12 – Thomas plots for the adsorption of MB onto GCLCB at different flow rates (10 mg/L initial MB concentration, 3 cm bed height and temperature 30±2 ˚C)

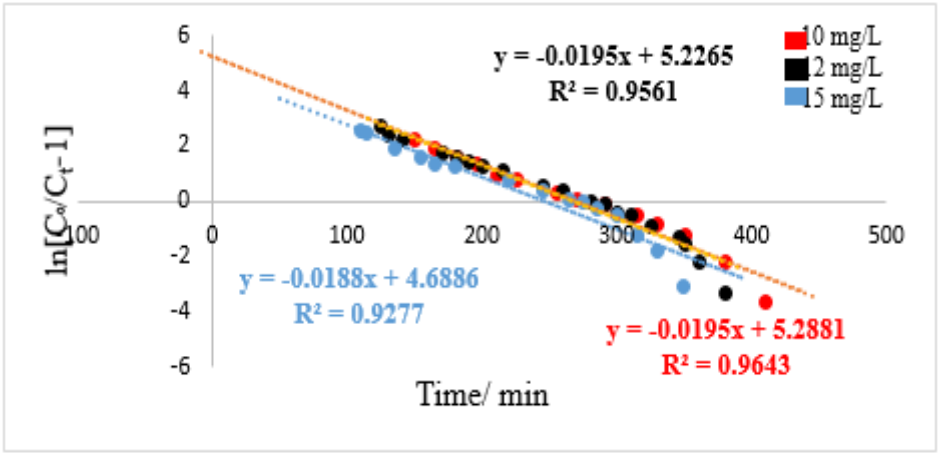

Figure 13 – Thomas plots for the adsorption of MB onto GCLCB at different initial concentrations (5 mL/min flow rate, 3 cm bed height and temperature 30±2 ˚C)

Table 4– Thomas kinetic model parameters at different conditions

Condition		Thomas kinetic model parameters		
		KT ($mLmin^{-1}mg^{-1}$)	$q_\circ$ (mg/g)	R^2
Bed height (cm)	1	3.970	3.38	0.8740
	2	2.930	4.04	0.9920
	3	1.950	4.13	0.9643
Flow rate (mL/min)	5	1.950	4.13	0.9643
	10	2.290	6.67	0.9195
	15	2.170	8.60	0.9375
Initial MB concentration (mg/L)	10	1.950	4.13	0.9643
	12	1.625	4.90	0.9561
	15	1.253	5.71	0.9277

According to the results as tabulated in table 4, values of maximum adsorption capacity, q_0 (mg/g) increased with increasing bed-height from 1 cm – 3 cm. But Thomas rate constant, decreased with increasing bed-height. Hence, the highest bed height is shown the better column performance. Similarly, as the initial dye concentration increases q° also increases, but k decreases. Both the rate constant, k and q° increased with increasing the flow rate. As the regression coefficient values, R^2, determined by the Thomas model are higher it can be concluded that the validity of the Thomas model for the studied column system.

Breakthrough curve analysis by the Yoon –Nelson model at different bed heights, inlet flow rates and initial MB concentrations

The experimental data were fitted with Yoon Nelson model to investigate the breakthrough characteristics of adsorption of MB onto the adsorbent. Yoon –Nelson plots at different bed heights, flow rates and initial concentrations are shown in figure 14, 15 and 16 respectively and kinetic parameters obtained from this model are shown in table 5.

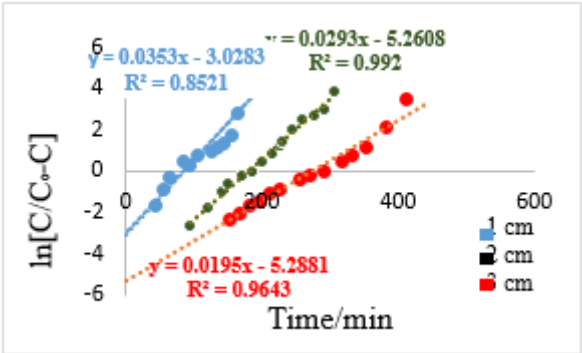

Figure 14 – Yoon –Nelson plots for the adsorption of MB onto GCLCB at different bed heights (initial MB dye concentration 10 mg/L, inlet flow rate 5 mg/L and temperature 30±2 °C).

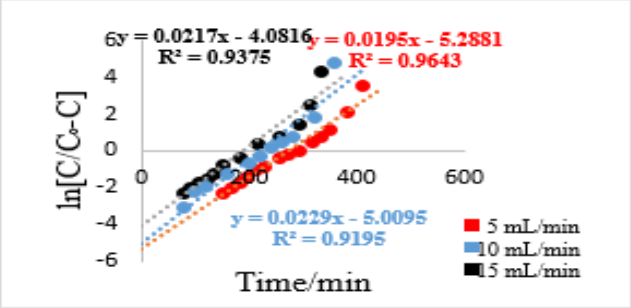

Figure 15 – Yoon –Nelson plots for the adsorption of MB onto GCLCB at different flow rates (10 mg/L initial MB concentration, 3 cm bed height and temperature 30±2 ˚C)

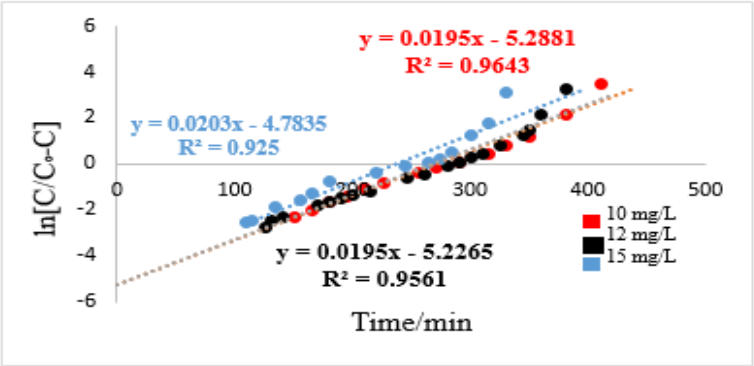

Figure 16 – Yoon –Nelson plots for the adsorption of MB onto GCLCB at different initial concentrations (5 mL/min flow rate, 3 cm bed height and temperature 30±2 ˚C)

Table 5– Yoon – Nelson kinetic model parameters

condition		Yoon – Nelson kinetic model parameters			
		K(min^{-1})	τ (min)	τ experiment (min)	R^2
Bed height(cm)	1	0.0353	85.79	69	0.874
	2	0.0293	179.55	183	0.992
	3	0.0195	271.18	281	0.9643
Flow rate(mL/min)	5	0.0195	271.18	281	0.9643
	10	0.0229	218.76	228	0.9195
	15	0.0217	188.09	195	0.9375
Initial concentration (mg/L)	10	0.0195	271.18	281	0.9643
	12	0.0195	268.03	280	0.9561
	15	0.203	235.64	265	0.9277

According to the results, τ value (the time required for 50% breakthrough) increases with the increment of bed height and decreases with the increment of flow rate and initial dye concentration. The predicted values of τ agreed quite well with the experimental data (τ experimental). Therefore, it is clear that Yoon –Nelson model fitted well with this column study and further, higher R^2 values support it.

Breakthrough curve analysis by the Adams – Bohart model at different bed heights, inlet flow rates and initial MB concentrations

Adams-Bohart plots at different bed heights, flow rates and initial MB concentrations are shown in figure 17,18 and 19 respectively and Adams – Bohart kinetic parameters; Bohart kinetic constant (k) and the saturation concentration (N^0) are shown in table 6.

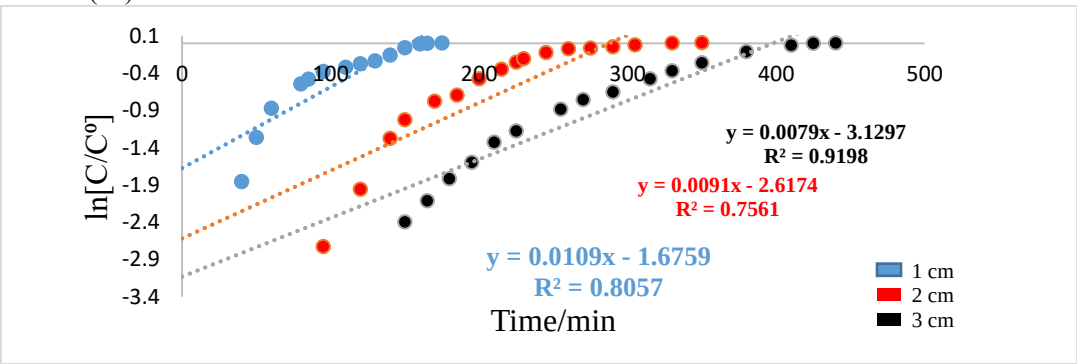

Figure 17– Adams – Bohart plot for the adsorption of MB onto GCLCB at different bed heights (initial MB dye concentration 10 mg/L, inlet flow rate 5 mg/L and temperature 30±2 ℃).

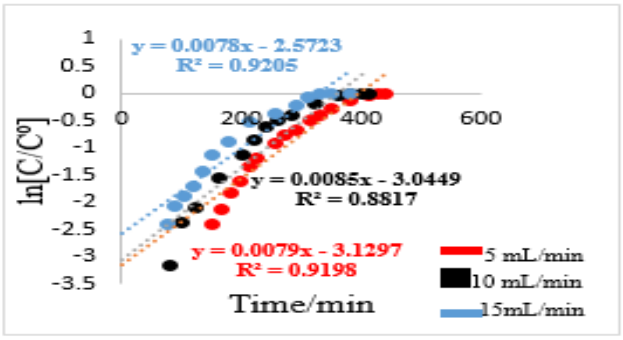

Figure 18 - Adams – Bohart plot for the adsorption of MB onto GCLCB at different flow rates (10 mg/L initial MB concentration, 3 cm bed height and temperature 30±2 ˚C)

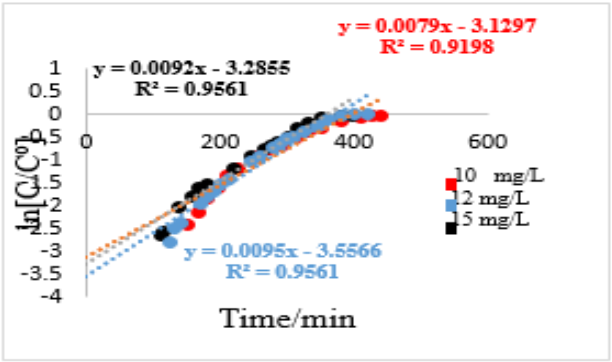

Figure 19 - Adams – Bohart plot for the adsorption of MB onto GCLCB at different initial concentrations (5 mL/min flow rate, 3 cm bed height and temperature 30±2 ˚C)

Table 6– Adams - Bohart kinetic parameters

condition		Adams - Bohart kinetic parameters		
		k ($Lmg^{-1}min^{-1}$)	N_0 (mg/ L)	R^2
Bed height(cm)	1	1.09×10^{-3}	1883.47	0.8057
	2	9.10×10^{-4}	1761.71	0.7561
	3	7.90×10^{-4}	1617.67	0.9198
Flow rate(mL/min)	5	7.90×10^{-4}	1617.67	0.9198
	10	8.50×10^{-4}	2931.46	0..8817
	15	7.80×10^{-4}	4045.33	0.9205
Initial concentration(mg/L)	10	7.90×10^{-4}	1617.67	0.9198
	12	7.08×10^{-4}	2050.37	0.9561
	15	5.20×10^{-4}	2579.96	0.9561

The values of k and N_0 decrease as the bed height increases but values of k decreases and N_0 increases with the increment of the initial MB concentration. A clear correlation is not observed between the flow rate and the values of k but N_0 increases as the flow rate increases. According to Table 6 as the R^2 values are lower than R^2 values obtained in Thomas and Yoon- Nelson models, it can be concluded that the lack of applicability of Adams - Bohart model for the studied column system.

CONCLUSION

Commercially available chitosan flakes were physically modified to CB. CBs were further chemically modified to GCLCB by using glutaraldehyde as the cross-linking agent. SEM and FTIR analyses were conducted for the characterization of chitosan beads and its GCLCB. The SEM analysis revealed that GCLCBs have highly porous structures with irregular surfaces. The effects of bed height, initial MB concentration and flow rate on the performance of fixed-bed column at 30 ± 2 ^{0}C were analyzed using BTCs. The highest experimental MB adsorption capacity of 225.47 mg/g was obtained at 3 cm bed height, 5 mL/min inlet flow rate and 12 mg/L of initial MB concentration. The breakthrough curves (BTCs) were analysed using three kinetic models, namely Thomas model, Yoon –Nelson model, and Adams – Bohart model. The application of Thomas model showed that the value of q° increased with increasing all three parameters, bed height, initial dye concentration and inlet flow rate. Yoon – Nelson model showed that the time required achieving 50% adsorbate breakthrough, τ fitted well with the experimental data (τ 50%) in the entire column system. Adams- Bohart model showed that Nº is increased with increasing initial dye concentration and flow rate and decreased with increasing bed height. Both the Thomas model, and Yoon –Nelson model showed good agreement with the experimental data. Further, the results revealed that the physically and chemically modified chitosan, GCLCB can be used as a natural adsorbent for the removal of MB from wastewater.

REFERENCES

1. Mathur, N. and Kumar, A., 2013. Physico-chemical characterization of industrial effluents contaminated soil of Sanganer. *Journal of Emerging Trends in Engineering and Applied Sciences*, *4*(2), pp.226-228.
2. Singare, S.S. and Dhabarde, S.S., 2014. Pollution discharge Scenario of Dyeing Industries along Dombivali Industrial Belt of Mumbai, India. *International Letters of Chemistry, Physics and Astronomy*, *3*, pp.48-55.
3. Gürses, M.S., Ahmet Gürses Metin Açıkyıldız Kübra Güneş.
4. Syeda, S.R., Ferdousi, S.A. and Ahmmed, K.T., 2012. De-colorization of textile wastewater by adsorption in a fluidized bed of locally available activated carbon. *Journal of Environmental Science and Health, Part A*, *47*(2), pp.210-220.
5. Mathur, N. and Bhatnagar, P., 2007. Mutagenicity assessment of textile dyes from Sanganer (Rajasthan). *Journal of Environmental Biology*, *28*(1), pp.123-126. [5] Ayed, L., Hkiri, N. & Hamdi, M., biomed-nedra asses (2018).
6. Muhammad, M.W., Latif, A. & Rahman, M. 2012, Fixed Bed Adsorption for Wastewater Treatment, (2012) pp.8-14
7. Asses, N., Ayed, L., Hkiri, N. and Hamdi, M., 2018. Congo Red Decolorization and Detoxification by Aspergillus niger: Removal Mechanisms and Dye Degradation Pathway. *BioMed research international*, *2018*.
8. Yagub, M.T., Sen, T.K., Afroze, S. and Ang, H.M., 2015. Fixed-bed dynamic column adsorption study of methylene blue (MB) onto pine cone. *Desalination and Water Treatment*, *55*(4), pp.1026-1039.
9. Mahaninia, M.H. and Wilson, L.D., 2016. Cross-linked chitosan beads for phosphate removal from aqueous solution. *Journal of Applied Polymer Science*, *133*(5).
10. Vieira, A.M.S., Vieira, M.F., Silva, G.F., Araújo, Á.A., Fagundes-Klen, M.R., Veit, M.T. and Bergamasco, R., 2010. Use of Moringa oleifera seed as a natural adsorbent for wastewater treatment. *Water, air, and soil pollution*, *206*(1-4), pp.273-281.
11. Galadima, L.G., Wasagu, R.S., Lawal, M., Aliero, A., Magajo, U.F. and Suleman, H., 2015. Biosorption activity of Nymphaea lotus (water lily). *The International Journal of Engineering and Science*, *4*(3), pp.66-70.
12. Abdelwahab, O., El Nemr, A., El Sikaily, A. and Khaled, A., 2005. Use of rice husk for adsorption of direct dyes from aqueous solution: a case study of Direct F. Scarlet. *Egyptian Journal of Aquatic Research*, *31*(1), pp.1-11.
13. Ojha, A., 2013. *Adsorption characteristics of jackfruit leaf powder (jlp) for the removal of dyes* (Doctoral dissertation).
14. Jóźwiak, T., Filipkowska, U., Bugajska, P. and Kalkowski, T., 2018. The Use of Coconut Shells for the Removal of Dyes from Aqueous Solutions. *Journal of Ecological Engineering*, *19*(4).
15. Abebe, L., Chen, X. and Sobsey, M., 2016. Chitosan coagulation to improve microbial and turbidity removal by ceramic water filtration for household drinking water treatment. *International journal of environmental research and public health*, *13*(3), p.269.
16. Vakili, M., Rafatullah, M., Salamatinia, B., Abdullah, A.Z., Ibrahim, M.H., Tan, K.B., Gholami, Z. and Amouzgar, P., 2014. Application of chitosan and its derivatives as adsorbents for dye removal from water and wastewater: A review. *Carbohydrate polymers*, *113*, pp.115-130.
17. Al-Manhel, A.J., Al-Hilphy, A.R.S. and Niamah, A.K., 2018. Extraction of chitosan, characterisation and its use for water purification. *Journal of the Saudi Society of Agricultural Sciences*, *17*(2), pp.186-190.
18. Elwakeel, K.Z., 2010. Environmental application of chitosan resins for the treatment of water and wastewater: a review. *Journal of dispersion science and technology*, *31*(3), pp.273-288.
19. Mustafa, A. and Cadar, E., 2015. Pharmaceutical Uses of Chitosan in the Medical Field. *European Journal of Interdisciplinary Studies*, *1*(3), pp.35-40.
20. Wang, X., Ma, J., Wang, Y. and He, B., 2002. Bone repair in radii and tibias of rabbits with phosphorylated chitosan reinforced calcium phosphate cements. *Biomaterials*, *23*(21), pp.4167-4176.
21. Miyazaki, S., Ishii, K. and Nadai, T., 1981. The use of chitin and chitosan as drug carriers. *Chemical and Pharmaceutical Bulletin*, *29*(10), pp.3067-3069.

22. Grumezescu, A.M. and Holban, A.M. eds., 2018. *Biopolymers for Food Design* (Vol. 20). Academic Press.
23. Bourtoom, T. and Chinnan, M.S., 2008. Preparation and properties of rice starch–chitosan blend biodegradable film. *LWT-Food science and Technology*, *41*(9), pp.1633-1641.
24. Aranaz, I., Acosta, N., Civera, C., Elorza, B., Mingo, J., Castro, C., Gandía, M. and Heras Caballero, A., 2018. Cosmetics and cosmeceutical applications of chitin, chitosan and their derivatives. *Polymers*, *10*(2), p.213.
25. Pokhrel, S., Yadav, P.N. and Adhikari, R., 2015. Applications of chitin and chitosan in industry and medical science: a review. *Nepal Journal of Science and Technology*, *16*(1), pp.99-104.
26. Kamel, S., El-Sakhawy, M. and Nada, A.M.A., 2004. Mechanical properties of the paper sheets treated with different polymers. *Thermochimica acta*, *421*(1-2), pp.81-85.
27. Pandey, P., Verma, M.K. and De, N., 2018. De N. Chitosan in agricultural context–a review. *Bulletin of Environment, Pharmacology and Life Sciences*, *7*(4), pp.87-96.
28. Gerente, C., Lee, V.K.C., Cloirec, P.L. and McKay, G., 2007. Application of chitosan for the removal of metals from wastewaters by adsorption—mechanisms and models review. *Critical reviews in environmental science and technology*, *37*(1), pp.41-127.
29. Miretzky, P. and Cirelli, A.F., 2011. Fluoride removal from water by chitosan derivatives and composites: a review. *Journal of Fluorine Chemistry*, *132*(4), pp.231-240.
30. Sahli, M.M., Annouar, S., Tahaikt, M., Mountadar, M., Soufiane, A. and Elmidaoui, A., 2007. Fluoride removal for underground brackish water by adsorption on the natural chitosan and by electrodialysis. *Desalination*, *212*(1-3), pp.37-45.
31. Chung, Y.C., Li, Y.H. and Chen, C.C., 2005. Pollutant removal from aquaculture wastewater using the biopolymer chitosan at different molecular weights. *Journal of environmental science and health*, *40*(9), pp.1775-1790.
32. Zemmouri, H., Drouiche, M., Sayeh, A., Lounici, H. and Mameri, N., 2013. Chitosan application for treatment of Beni-Amrane's water dam. *Energy Procedia*, *36*, pp.558-564.
33. Vieira, R.S. and Beppu, M.M., 2006. Interaction of natural and crosslinked chitosan membranes with Hg (II) ions. *Colloids and Surfaces A: Physicochemical and Engineering Aspects*, *279*(1-3), pp.196-207.
34. Hsien, T.Y. and Rorrer, G.L., 1997. Heterogeneous cross-linking of chitosan gel beads: kinetics, modeling, and influence on cadmium ion adsorption capacity. *Industrial & engineering chemistry research*, *36*(9), pp.3631-3638.
35. Hasan, S., Krishnaiah, A., Ghosh, T.K., Viswanath, D.S., Boddu, V.M. and Smith, E.D., 2006. Adsorption of divalent cadmium (Cd (II)) from aqueous solutions onto chitosan-coated perlite beads. *Industrial & engineering chemistry research*, *45*(14), pp.5066-5077.
36. Zhao, L.M., Shi, L.E., Zhang, Z.L., Chen, J.M., Shi, D.D., Yang, J. and Tang, Z.X., 2011. Preparation and application of chitosan nanoparticles and nanofibers. *Brazilian Journal of Chemical Engineering*, *28*(3), pp.353-362.
37. Chang, Y.C., Chang, S.W. and Chen, D.H., 2006. Magnetic chitosan nanoparticles: Studies on chitosan binding and adsorption of Co (II) ions. *Reactive and Functional Polymers*, *66*(3), pp.335-341.
38. Agboh, O.C. and Qin, Y., 1997. Chitin and chitosan fibers. *Polymers for Advanced Technologies*, *8*(6), pp.355-365.
39. Peirano, F., Vincent, T., Quignard, F., Robitzer, M. and Guibal, E., 2009. Palladium supported on chitosan hollow fiber for nitrotoluene hydrogenation. *Journal of Membrane Science*, *329*(1-2), pp.30-45.
40. Denkbaş, E.B. and Odabaşi, M., 2000. Chitosan microspheres and sponges: preparation and characterization. *Journal of Applied Polymer Science*, *76*(11), pp.1637-1643.
41. Fernandes Queiroz, M., Melo, K., Sabry, D., Sassaki, G. and Rocha, H., 2015. Does the use of chitosan contribute to oxalate kidney stone formation?. *Marine drugs*, *13*(1), pp.141-158.
42. Auta, M. and Hameed, B.H., 2014. Chitosan–clay composite as highly effective and low-cost adsorbent for batch and fixed-bed adsorption of methylene blue. *Chemical Engineering Journal*, *237*, pp.352-361.
43. López-Cervantes, J., Sánchez-Machado, D.I., Sánchez-Duarte, R.G. and Correa-Murrieta, M.A., 2018. Study of a fixed-bed column in the adsorption of an azo dye from an aqueous medium using a chitosan–glutaraldehyde biosorbent. *Adsorption Science & Technology*, *36*(1-2), pp.215-232.
44. Crhribi, A. and Chlendi, M., 2011. Modeling of fixed bed adsorption: application to the adsorption of an

organic dye. *Asian J. Textile*, *1*, pp.161-171.

45. Sadaf, S. and Bhatti, H.N., 2014. Evaluation of peanut husk as a novel, low cost biosorbent for the removal of Indosol Orange RSN dye from aqueous solutions: batch and fixed bed studies. *Clean Technologies and Environmental Policy*, *16*(3), pp.527-544.
46. Chowdhury, Z.Z., Zain, S.M., Rashid, A.K., Rafique, R.F. and Khalid, K., 2012. Breakthrough curve analysis for column dynamics sorption of Mn (II) ions from wastewater by using Mangostana garcinia peel-based granular-activated carbon. *Journal of chemistry*, *2013*.
47. Lim, A.P. and Aris, A.Z., 2014. Continuous fixed-bed column study and adsorption modeling: Removal of cadmium (II) and lead (II) ions in aqueous solution by dead calcareous skeletons. *Biochemical Engineering Journal*, *87*, pp.50-61.